

# Creep of Concrete Core and Time-Dependent Non-Linear Behaviour and Buckling of Shallow Concrete-Filled Steel Tubular Arches

K. Luo<sup>1</sup>, Y. L. Pi<sup>1</sup>, W. Gao<sup>1</sup>, and M. A. Bradford<sup>1</sup>

**Abstract:** This paper presents a theoretical analysis for the time-dependent non-linear behaviour and buckling of shallow concrete-filled steel tubular (CFST) arches under a sustained central concentrated load. The virtual work method is used to establish the differential equations of equilibrium for the time-dependent behaviour and buckling analyses of shallow CFST arches, and the age-adjusted effective modulus method is adopted to model the creep behaviour of the concrete core. Analytical solutions of time-dependent displacements and internal forces of shallow CFST arches are derived. It has been found that under a sustained central concentrated load, the deformations and bending moments in a shallow CFST arch are time-dependent and they increase with time significantly owing to the creep of the concrete core, which lead to the change of equilibrium configurations of the arch with time. When the time is sufficiently long, the stable equilibrium configuration of the arch under the sustained load in the short-term continues to change until its buckling configuration corresponding to the sustained load is attained. In this case, the arch may buckle in a bifurcation mode or a limit point instability mode. The analytical solution of the prebuckling structural life time is also derived. Comparisons of the analytical solutions with the finite element results show that the analytical solutions of the present study are effective and accurate.

**Keywords:** CFST arch, creep and shrinkage, non-linear, buckling.

## 1 Introduction

Applications of concrete filled steel tubular (CFST) arches are increasing in engineering structures, particularly in bridge constructions [Chen (2000); Pi, Liu, Bradford, and Zhang (2012)]. A CFST section is composed of well bonded steel tube and concrete core as shown in Fig. 1 and is capable to provide the required

---

<sup>1</sup> School of Civil and Environmental Engineering, University of New South Wales, Sydney, NSW 2052, AUSTRALIA.

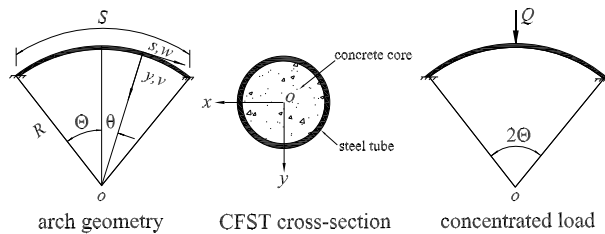


Figure 1: Concrete filled steel tubular arch.

structural stiffness and strength. The steel tube confines the concrete core with significant improvement of load-carrying capacity and ductility while the concrete core restrains the steel tube from local buckling. However, the visco-elastic effects of creep and shrinkage of concrete core are inevitable in the long term for CFST arches. When a CFST arch is subjected to a sustained load, the creep of the concrete core will lead to the increase of its deformations with time and the deformations may be significant, while the shrinkage strain may also develop even when the arch is not subjected to any load [Gilbert and Ranzi (2011); Bazant and Cedolin (2003)]. Hence, an investigation of significant effects of creep and shrinkage of the concrete core on the time-dependent structural behaviour of CFST arches is much needed.

Investigations on the visco-elastic effects of creep and shrinkage of the concrete core have been focused on straight CFST members. Uy (2001) studied the long-term effects in short concrete-filled steel box columns under sustained loading, while Han, Yang, and Liu (2004) investigated the behaviour of concrete-filled steel tubular columns with rectangular section under long-term loading. It has been shown that the short-term structural behaviour of CFST arches is quite different from that of straight CFST members [Pi, Liu, Bradford, and Zhang (2012)]. Hence, it is anticipated the long-term behaviour of CFST arches differs from that of straight CFST members. When a CFST arch is subjected to a sustained transverse load, the load will produce axial compressive and bending actions in the arch and so the creep and shrinkage behaviour of the arch is expected to be much complicated than that of straight CFST members. For example, although a CFST arch does not buckle in short term when the applied load is lower than the corresponding buckling load, it may buckle in the long-term under the sustained load because the visco-elastic effects of creep and shrinkage of the concrete core changes its time-dependent equilibrium configuration, which may attain the buckling configuration of the arch [Bradford, Pi, and Qu (2011)] when the time is sufficiently long. Hence, investigation of the time-dependent behaviour of CFST arches is desirable. However, in the open literature, studies of the time-dependent structural behaviour and

buckling of shallow CFST arches due to the creep and shrinkage of the concrete core seem to be scarce. Bradford, Pi, and Qu (2011) studied the time-dependent in-plane behaviour and buckling of concrete-filled steel tubular arches by using linear and eigenvalue analysis, while Pi, Bradford, and Qu (2011) investigated the long-term non-linear behaviour and buckling of shallow concrete-filled steel tubular arches under a sustained uniform radial load.

In the construction practice, many CFST arches have rise-to-span ratios in the range from 1/10 to 1/4 and so they should be considered as shallow arches [Pi, Liu, Bradford, and Zhang (2012)]. Hence, investigation of the time-dependent behaviour of shallow CFST arches is particularly important. It has been shown that the structural behaviour of shallow arches is quite non-linear and the non-linear relationship between the external load and the internal non-uniform bending and axial compressive actions is very much different under different loading cases [Pi, Bradford, and Uy (2002), Pi, Bradford, and Tin-Loi (2007), Pi and Bradford (2009)]. When an arch is subjected to a central concentrate load, the bending action is relatively high and compressive action is relatively low. It is not known how these differences influence the non-linear time-dependent behaviour and buckling of shallow CFST arches under a sustained central concentrated load, and whether or not the linear analysis that is currently used for the time-dependent analysis of straight CFST members can correctly predict the time-dependent deformations of shallow CFST arches. It is also not known how the creep of the concrete core under the sustained central concentrated load induces the time-dependent buckling of shallow CFST arches.

This paper, therefore, aims to investigate the time-dependent non-linear behaviour and buckling of shallow CFST arches under a central concentrated load, to derive analytical solutions for their time-dependent non-linear deformations, internal forces and buckling, and to determine their structural life time prior to the buckling. To investigate the effects of the creep and shrinkage of concrete core, it is important to use an efficient and accurate method to describe the the creep and shrinkage of concrete. It is known that a number of methods have been proposed and used for the the creep and shrinkage of the concrete [Bazant and Cedolin (2003), Abdulrazeg, Noorzaei, Khanehzaei, Jaafar, and Mohammed (2010), Ferretti and Di Leo (2008)]. Among these methods, the age-adjusted effective modulus method recommended by ACI Committee-209 and Australia design code for the concrete structures AS3600 are commonly considered to be efficient and accurate in evaluating the time-dependent behaviour of the concrete and it could conveniently be incorporated into the structural analysis [Gilbert and Ranzi (2011); Bazant and Cedolin (2003); Wang, Bradford, and Gilbert (2005); Bazant (1972)]. Algebraic formulas used in this method can be effective and practicable in modeling creep and shrink-

age of concrete core, so the age-adjusted effective modulus method is used in this investigation.

## 2 Time-dependent linear elastic analysis

Before dealing with the non-linear analysis, the time-dependent linear elastic analysis is herein conducted for the subsequent comparisons. The following assumptions need to be adopted for both the linear and non-linear analysis: (1) deformations of CFST arch are elastic and satisfy the Euler-Bernoulli hypothesis, i.e. the cross-section remains plane and perpendicular to the arch axis during deformation; (2) the dimensions of the cross-section are much smaller than the length and radius of the arch so that the arches are sufficiently slender; and (3) the cohesion and adhesion of two different material components are fully bonded.

For the linear analysis, the strain of an arbitrary point of the cross-section can be expressed as

$$\varepsilon = \tilde{w}' - \tilde{v} - \frac{y(\tilde{v}'' + \tilde{w}')}{R}, \quad (1)$$

where  $\tilde{v} = v/R$  and  $\tilde{w} = w/R$ ,  $v$  and  $w$  are the radial and axial displacements in the directions of the axes  $oy$  and  $os$ ,  $y$  locates the point in the principal axis  $oy$  and while  $\theta$  sweeps from the left to right in the angular coordinate, and  $( )'$  and  $( )''$  denote  $d( )/d\theta$  and  $d^2( )/d\theta^2$ .

According to the third assumption, the deformations of each component should be compatible with each other, so their membrane strains and also the strains at the interface are identical. However, due to different Young's moduli and the effects of creep and shrinkage in concrete core, the stress  $\sigma_s$  in the steel tube and the stress  $\sigma_c$  in the concrete core are different and they are given by

$$\sigma_s = E_s \varepsilon \quad \text{and} \quad \sigma_c = E_{ec}(\varepsilon + \varepsilon_{sh}) \quad (2)$$

where  $E_s$  is Young's modulus of steel and  $E_{ec}$  is the age-adjusted effective modulus of concrete core defined as [Gilbert and Ranzi (2011); Bazant (1972)]

$$E_{ec}(t, t_0) = \frac{E_c}{1 + \chi(t, t_0)\phi(t, t_0)}, \quad (3)$$

in which  $\phi(t, t_0)$  is the creep coefficient and  $\chi(t, t_0)$  is the ageing coefficient and they are given by [Gilbert and Ranzi (2011); Branson (1977)]

$$\phi(t, t_0) = \left[ \frac{(t - t_0)^{0.6}}{10 + (t - t_0)^{0.6}} \right] \phi_u \quad \text{and} \quad \chi(t, t_0) = 1 - \frac{(1 - \chi^*)(t - t_0)}{20 + (t - t_0)} \quad (4)$$

respectively, where  $\phi_u$  is the final creep coefficient (the value of  $\phi(t, t_0)$  when  $t \rightarrow \infty$ ) and given by

$$\begin{aligned} \phi_u &= 1.25t_0^{-0.118} \phi_{\infty,7}, \chi^* = \frac{k_1 t_0}{k_2 + t_0}, \\ k_1 &= 0.78 + 0.4e^{-1.33\phi_{\infty,7}}, k_2 = 0.16 + 0.8e^{-1.33\phi_{\infty,7}}, \end{aligned} \quad (5)$$

and  $\epsilon_{sh}$  is the shrinkage strain of the concrete and can be expressed by ACI Committee-209 and Australian design code for concrete structures AS3600 as

$$\epsilon_{sh} = \left( \frac{t}{t+d} \right) \epsilon_{sh}^* \quad (6)$$

in which  $t$  is the time in days. Because of the confinement of the steel tube, egress of the moisture in the concrete core is prevented and  $d = 35$  days for moist curing can be used for the concrete core of CFST members.  $\epsilon_{sh}^*$  is the final shrinkage strain that is the value of  $\epsilon_{sh}$  when  $t \rightarrow \infty$ .

The empirical values for the final shrinkage strain  $\epsilon_{sh}^*$  and the final creep coefficient  $\phi_u$  of CFST columns were proposed from experimental studies [Zhong (1994); Terrey, Bradford, and Gilbert (1994); Uy (2001); Han, Yang, and Liu (2004)]. However, to some extent, these experimental data cannot be used directly, but they can be used to derive the empirical values for the final shrinkage strain and the final creep coefficient through a time-dependent analysis. For example, the empirical value of the final shrinkage strain  $\epsilon_{sh}^* = 340 \times 10^{-6}$  (the value when  $t \rightarrow \infty$ ) and the final creep coefficient  $\phi_u = 2.29$  can be derived from Uy (2001) and these values are used in this investigation.

The differential equations of the time-dependent equilibrium for the CFST arch under a central concentrated load can be derived from the virtual work principle, which can be stated as that

$$\delta W = \int_{V_s} \sigma_s \delta \epsilon dV + \int_{V_c} \sigma_c \delta \epsilon dV - \int_{-\theta}^{\theta} QR \cdot \text{Dirac}(\theta) \delta \tilde{v} d\theta = 0 \quad (7)$$

holds for all arbitrary variations of the admissible deformations  $\delta \tilde{v}$  and  $\delta \tilde{w}$ , where  $V_s$  and  $V_c$  are the volume of the steel tube and concrete core respectively,  $\delta(\ )$  denotes the Lagrange operator of simultaneous variations, and  $\text{Dirac}(\theta)$  is the Dirac delta function defined by

$$\text{Dirac}(\theta) = \begin{cases} +\infty, & \theta = 0 \\ 0, & \theta \neq 0 \end{cases} \quad \text{and} \quad \int_{-\infty}^{\infty} \text{Dirac}(\theta) d\theta = 1, \quad (8)$$

and it has the property

$$\int_{-\infty}^{\infty} \text{Dirac}(\theta) f(\theta) d\theta = f(0). \quad (9)$$

By substituting Eqs. (1) and (2), the statement of the principle of virtual work given by Eq. (7) becomes

$$\delta W = \int_{-\Theta}^{\Theta} \{[-NR(\delta\tilde{w}' - \delta\tilde{v}) - M(\delta\tilde{v}'' + \delta\tilde{w}')] - QR \cdot \text{Dirac}(\theta)\delta\tilde{v}\} d\theta = 0, \quad (10)$$

where the axial compressive force  $N$  is given by

$$N = - \int_{A_s} \sigma_s dA - \int_{A_c} \sigma_c dA = -(A_s E_s + A_c E_{ec})(\tilde{w}' - \tilde{v}) - A_c E_{ec} \varepsilon_{sh} \quad (11)$$

and the bending moment  $M$  is given by

$$M = \int_{A_s} \sigma_{sy} dA + \int_{A_c} \sigma_{cy} dA = -(E_s I_s + E_{ec} I_c) \frac{\tilde{v}'' + \tilde{w}'}{R}, \quad (12)$$

where  $A_c$  and  $A_s$ , and  $I_c$  and  $I_s$ , are the area and second moment of area of the concrete core and steel tube respectively.

Integrating Eq. (10) by parts leads to the differential equations of equilibrium as

$$r_e^2 (\tilde{v}^{iv} + \tilde{w}''') - R^2 (\tilde{w}' - \tilde{v} + \frac{A_c E_{ec} \varepsilon_{sh}}{A_s E_s + A_c E_{ec}}) - \frac{QR^2 \cdot \text{Dirac}(\theta)}{A_s E_s + A_c E_{ec}} = 0 \quad (13)$$

in the radial direction, and

$$r_e^2 (\tilde{v}''' + \tilde{w}'') + R^2 (\tilde{w}'' - \tilde{v}') = 0 \quad (14)$$

in the axial direction; and leads to the static boundary conditions for pin-ended arches as

$$\tilde{v}'' + \tilde{w}' = 0 \quad \text{at } \theta = \pm \Theta, \quad (15)$$

where the time-dependent radius of gyration of the effective cross-section  $r_e$  about its major principal axis is defined by

$$r_e = \sqrt{\frac{E_s I_s + E_{ec} I_c}{A_s E_s + A_c E_{ec}}} \quad (16)$$

The essential kinematic boundary conditions are

$$\tilde{v} = 0 \quad \text{and} \quad \tilde{w} = 0 \quad \text{at } \theta = \pm \Theta \quad (17)$$

for pin-ended arches, and

$$\tilde{v} = 0, \quad \tilde{v}' = 0 \quad \text{and} \quad \tilde{w} = 0 \quad \text{at } \theta = \pm \Theta \quad (18)$$

for fixed arches.

The time-dependent radial and axial displacements  $\tilde{v}$  and  $\tilde{w}$  for pin-ended arches can then be obtained by solving Eqs. (13) and (14) simultaneously and using the boundary conditions given by Eqs. (15) and (17) as

$$\tilde{v} = Q \left\{ (D_1 + D_4) \cos \theta + D_2 \theta \sin \theta - D_3 + \frac{H(\theta)(r_e^2 + R^2)}{4(E_s I_s + E_{ec} I_c)} (\sin \theta - \theta \cos \theta) \right\} + \frac{A_c E_{ec} \epsilon_{sh} \Gamma_1(\theta)}{(A_s E_s + A_c E_{ec}) \Phi_P}, \quad (19)$$

and

$$\tilde{w} = Q \left\{ D_4 \sin \theta - D_2 \theta \cos \theta - D_3 \theta + \frac{H(\theta)[2R^2(1 - \cos \theta) - (R^2 + r_e^2)\theta \sin \theta]}{4(E_s I_s + E_{ec} I_c)} \right\} + \frac{A_c E_{ec} \epsilon_{sh} \Gamma_2(\theta)}{(A_s E_s + A_c E_{ec}) \Phi_P}, \quad (20)$$

with

$$\Gamma_1(\theta) = (\cos \theta - \cos \Theta) [(R^2 - r_e^2) \sin \Theta - 2R^2 \Theta \cos \Theta] + (R^2 + r_e^2) (\Theta - \Theta \cos \theta \cos \Theta - \theta \sin \theta \sin \Theta)$$

and

$$\Gamma_2(\theta) = (R^2 + r_e^2) (\theta \cos \theta \sin \Theta - \Theta \cos \Theta \sin \theta) + 2R^2 \cos \Theta (\theta \sin \Theta - \Theta \sin \theta),$$

where the step function  $H(\theta)$  is defined as

$$H(\theta) = \begin{cases} -1 & \text{when } \theta < 0 \\ 1 & \text{when } \theta \geq 0 \end{cases}, \quad (21)$$

and the coefficients  $D_1$ ,  $D_2$ ,  $D_3$  and  $D_4$  are given by

$$D_1 = \frac{(r_e^2 - R^2) \Xi_1}{4(E_s I_s + E_{ec} I_c) \Phi_P}, \quad D_2 = \frac{(R^2 + r_e^2) \Xi_1}{4(E_s I_s + E_{ec} I_c) \Phi_P}, \quad (22)$$

$$D_3 = \frac{R^2 [2R^2 \cos \Theta (\cos \Theta - 1) + (R^2 + r_e^2) \Theta \sin \Theta]}{2(E_s I_s + E_{ec} I_c) \Phi_P}, \quad (23)$$

and

$$D_4 = \frac{(R^2 + r_e^2) [\Theta^2 (3R^2 + r_e^2) - 2R^2 \Theta \sin \Theta]}{4(E_s I_s + E_{ec} I_c) \Phi_P} + \frac{2R^2 \cos \Theta [(3R^2 - r_e^2) (1 - \cos \Theta) - 2R^2 \Theta \sin \Theta]}{4(E_s I_s + E_{ec} I_c) \Phi_P}, \quad (24)$$

with the time-dependent parameters  $\Xi_1$  and  $\Phi_P$  being given by

$$\Xi_1 = [2R^2 \cos \Theta (1 - \cos \Theta - \Theta \sin \Theta) + (R^2 - r_e^2) \sin^2 \Theta] \quad (25)$$

and

$$\Phi_P = R^2 (\Theta - 3 \cos \Theta \sin \Theta + 2\Theta \cos^2 \Theta) + r_e^2 (\Theta + \cos \Theta \sin \Theta). \quad (26)$$

The radial and axial displacements for fixed arches can be obtained in the same way by considering the boundary condition Eq. (18) as

$$\begin{aligned} \tilde{v} = & Q \left\{ (D_1 + D_4) \cos \theta + D_2 \theta \sin \theta + D_3 + \frac{H(\theta)(r_e^2 + R^2)}{4(E_s I_s + E_{ec} I_c)} (\sin \theta - \theta \cos \theta) \right\} \\ & + \frac{A_c E_{ec} \varepsilon_{sh} \Theta (R^2 + r_e^2) \Gamma_3(\theta)}{(A_s E_s + A_c E_{ec}) \Phi_F}, \end{aligned} \quad (27)$$

and

$$\begin{aligned} \tilde{w} = & Q \left\{ D_4 \sin \theta - D_2 \theta \cos \theta + D_3 \theta + \frac{H(\theta)[2R^2(1 - \cos \theta) - (R^2 + r_e^2)\theta \sin \theta]}{4(E_s I_s + E_{ec} I_c)} \right\} \\ & + \frac{A_c E_{ec} \varepsilon_{sh} \Gamma_4(\theta)}{(A_s E_s + A_c E_{ec}) \Phi_F}, \end{aligned} \quad (28)$$

with

$$\Gamma_3(\theta) = \Theta - \Theta \cos \theta \cos \Theta - \cos \theta \sin \Theta + \cos \Theta \sin \Theta - \theta \sin \theta \sin \Theta$$

and

$$\Gamma_4(\theta) = \Theta (R^2 + r_e^2) (\theta \sin \Theta \cos \theta - \Theta \sin \theta \cos \Theta) + 2R^2 \sin \Theta (\theta \sin \Theta - \Theta \sin \theta),$$

where the coefficients  $D_1$ ,  $D_2$ ,  $D_3$  and  $D_4$  are given by

$$D_1 = \frac{(r_e^2 - R^2) \Xi_2}{4(E_s I_s + E_{ec} I_c) \Phi_F}, \quad D_2 = \frac{(R^2 + r_e^2) \Xi_2}{4(E_s I_s + E_{ec} I_c) \Phi_F}, \quad (29)$$

$$D_3 = \frac{R^2 (R^2 + r_e^2) (\Theta - \sin \Theta) (\cos \Theta - 1)}{2(E_s I_s + E_{ec} I_c) \Phi_F}, \quad (30)$$

and

$$D_4 = \frac{2R^2 (\cos \Theta - 1) [\Theta (R^2 + r_e^2) (\cos \Theta + 2) - 2R^2 \sin \Theta]}{4(E_s I_s + E_{ec} I_c) \Phi_F} + \frac{\Theta^3 (R^2 + r_e^2)^2}{4(E_s I_s + E_{ec} I_c) \Phi_F} \quad (31)$$

with the time-dependent parameters  $\Xi_2$  and  $\Phi_F$  being given by with

$$\Xi_2 = (\cos \Theta - 1)[\Theta(R^2 + r_e^2)(\cos \Theta + 1) - 2R^2 \sin^2 \Theta] \quad (32)$$

and

$$\Phi_F = \Theta(R^2 + r_e^2)(\cos \Theta \sin \Theta + \Theta) - 2R^2 \sin^2 \Theta. \quad (33)$$

The time-dependent axial compressive force  $N$  and bending moment  $M$  can then be obtained as

$$\begin{aligned} N &= -(A_s E_s + A_c E_{ec})(\tilde{w}' - \tilde{v}) - A_c E_{ec} \varepsilon_{sh} \\ &= Q \cos \theta \Xi_3 + \frac{QH(\theta) \sin \theta}{2} - \frac{2r_e^2 \cos \theta \sin \theta}{\Phi_P} A_c E_{ec} \varepsilon_{sh} \end{aligned} \quad (34)$$

with

$$\Xi_3 = \frac{[2 \cos \Theta (1 - \Theta \sin \Theta - \cos \Theta) R^2 + \sin^2 \Theta (R^2 - r_e^2)]}{2\Phi_P},$$

and

$$M = -(E_s I_s + E_{ec} I_c) \frac{\tilde{w}'' + \tilde{w}'}{R} = QR \Xi_4 - NR - \frac{2Rr_e^2 \sin \Theta \cos \Theta}{\Phi_P} A_c E_{ec} \varepsilon_{sh} \quad (35)$$

with

$$\Xi_4 = \frac{[2 \cos \Theta (\cos \Theta - 1) R^2 + \Theta \sin \Theta (R^2 + r_e^2)]}{2\Phi_P}$$

for pin-ended arches; and

$$\begin{aligned} N &= -(A_s E_s + A_c E_{ec})(\tilde{w}' - \tilde{v}) - A_c E_{ec} \varepsilon_{sh} \\ &= Q \cos \theta \Xi_5 + \frac{QH(\theta) \sin \theta}{2} - \frac{2r_e^2 \Theta \sin \Theta \cos \theta}{\Phi_F} A_c E_{ec} \varepsilon_{sh} \end{aligned} \quad (36)$$

with

$$\Xi_5 = \frac{(\cos \Theta - 1)[(R^2 + r_e^2)\Theta(1 + \cos \Theta) - 2R^2 \sin \Theta]}{2\Phi_F},$$

and

$$M = -(E_s I_s + E_{ec} I_c) \frac{\tilde{w}'' + \tilde{w}'}{R} = QR \Xi_6 - NR - \frac{2Rr_e^2 \sin^2 \Theta}{\Phi_F} A_c E_{ec} \varepsilon_{sh} \quad (37)$$

with

$$\Xi_6 = \frac{(R^2 + r_e^2)(\cos \Theta - 1)(\sin \Theta - \Theta)}{2\Phi_F}$$

for fixed arches.

### 3 Time-dependent non-linear elastic analysis

To account for the non-linearity resulted from creep and shrinkage of the concrete core, the derivation of the differential equations of equilibrium for shallow CFST arches needs to consider non-linear longitudinal normal strain-displacement relationship and the non-linear longitudinal normal strain  $\varepsilon$  of an arbitrary point in the cross-section of shallow CFST arches can then be expressed as [Pi, Bradford, and Uy (2002); Pi and Trahair (1998)]

$$\varepsilon = \tilde{w}' - \tilde{v} + \frac{1}{2}(\tilde{v}')^2 - \frac{y\tilde{v}''}{R}. \quad (38)$$

For shallow arches, the effects of the axial deformations on the radial deformations are so small that they can be ignored in the analysis [Pi, Bradford, and Uy (2002); Pi and Trahair (1998); Pi, Bradford, Tin-Loi, and Gilbert (2007)].

Substituting Eqs. (2) and (38) into the statement of the principle of virtual work given by Eq. (7) results in the new form as

$$\delta W = \int_{-\Theta}^{\Theta} \{[-NR(\delta\tilde{w}' - \delta\tilde{v} + \tilde{v}'\delta\tilde{v}') - M\delta\tilde{v}''] - QR \cdot \text{Dirac}(\theta)\delta\tilde{v}\} d\theta = 0, \quad (39)$$

where the axial compressive force  $N$  is given by

$$N = - \int_{A_s} \sigma_s dA - \int_{A_c} \sigma_c dA = -(A_s E_s + A_c E_{ec})[\tilde{w}' - \tilde{v} + \frac{1}{2}(\tilde{v}')^2] - A_c E_{ec} \varepsilon_{sh}, \quad (40)$$

and the bending moment  $M$  is given by

$$M = \int_{A_s} \sigma_s y dA + \int_{A_c} \sigma_c y dA = -(E_s I_s + E_{ec} I_c) \frac{\tilde{v}''}{R}. \quad (41)$$

Integrating Eq. (39) by parts leads to the differential equations of equilibrium for the analysis of the time-dependent behaviour of CFST arches as

$$N' = 0 \quad (42)$$

in the axial direction, and

$$-M'' + NR\tilde{v}'' + NR - QR \cdot \text{Dirac}(\theta) = 0 \quad (43)$$

in the radial direction; and leads to the static boundary conditions for pin-ended arches as

$$M = 0 \text{ at } \theta = \pm \Theta. \quad (44)$$

From Eq. (42), the axial compressive force  $N$  is constant along the length of arch. Substituting the constant axial compressive force  $N$  and the expression for  $M$  given by Eq. (41) into Eq. (43) leads to

$$\frac{\tilde{v}^{iv}}{\mu_e^2} + \tilde{v}'' = -1 + \frac{QR^2 \cdot \text{Dirac}(\theta)}{\mu_e^2(E_s I_s + E_{ec} I_c)}, \quad (45)$$

where  $\mu_e$  is a time-dependent dimensionless axial force parameter defined by

$$\mu_e^2 = \frac{NR^2}{E_s I_s + E_{ec} I_c} \quad (46)$$

By using the kinematic boundary conditions that  $\tilde{v} = \tilde{v}'' = 0$  at  $\theta = \pm \Theta$  for pin-ended arches, and that  $\tilde{v} = \tilde{v}' = 0$  at  $\theta = \pm \Theta$  for fixed arches. The solutions of the radial displacement can be obtained from Eq. (45) as

$$\begin{aligned} \tilde{v} = \frac{1}{\mu_e^2} \left\{ 1 - \frac{\cos \mu_e \theta}{\cos \beta_e} + \frac{1}{2} [\beta_e^2 - (\mu_e \theta)^2] \right\} \\ + \frac{\bar{Q}}{\mu_e^2 \beta_e} \left\{ \tan \beta_e \cos \mu_e \theta - \beta_e - H(\theta)(\sin \mu_e \theta - \mu_e \theta) \right\} \end{aligned} \quad (47)$$

for pin-ended arches; and

$$\begin{aligned} \tilde{v} = \frac{1}{\mu_e^2} \left\{ \frac{\beta_e (\cos \beta_e - \cos \mu_e \theta)}{\sin \beta_e} + \frac{1}{2} [\beta_e^2 - (\mu_e \theta)^2] \right\} \\ + \frac{\bar{Q}}{\mu_e^2 \beta_e} \left\{ \tan\left(\frac{\beta_e}{2}\right) (\cos \mu_e \theta + 1) - \beta_e - H(\theta)(\sin \mu_e \theta - \mu_e \theta) \right\} \end{aligned} \quad (48)$$

for fixed arches, where  $\beta_e = \mu_e \Theta$ , and  $\bar{Q}$  is the dimensionless load defined by

$$\bar{Q} = \frac{QR^2 \Theta}{2(E_{ec} I_c + E_s I_s)} = \frac{\pi^2 Q}{2\Theta N_P} = \frac{(1.4303\pi)^2 Q}{2\Theta N_F}, \quad (49)$$

in which  $N_P$  and  $N_F$  are the second mode buckling load of a pin-ended and fixed CFST column about its major axis under uniform axial compression, respectively and they are given by

$$N_P = \frac{\pi^2 (E_s I_s + E_{ec} I_c)}{(S/2)^2} \quad \text{and} \quad N_F = \frac{(1.4303\pi)^2 (E_s I_s + E_{ec} I_c)}{(S/2)^2}. \quad (50)$$

It can be seen from Eqs. (47) and (48) that the radial displacement  $\tilde{v}$  is a non-linear function of the dimensionless time-dependent axial force parameter  $\mu_e$  and the sustained concentrated load  $\bar{Q}$ .

#### 4 Time-dependent non-linear equilibrium equation between internal and external forces

The constant axial force obtained from Eq. (42) should be equal to the average value of  $N$  over the entire arch calculated from Eq. (40) as

$$N = \frac{1}{2\Theta} \int_{-\Theta}^{\Theta} -\{(A_s E_s + A_c E_{ec})[\tilde{w}' - \tilde{v} + \frac{1}{2}(\tilde{v}')^2] - A_c E_{ec} \epsilon_{sh}\} d\theta. \quad (51)$$

Substituting Eqs. (47) and (48) into Eq. (51) with the boundary condition that  $\tilde{w} = 0$  at  $\theta = \pm \Theta$  leads to a non-linear equation of equilibrium between the axial force parameter  $\beta_e$  and the dimensionless sustained concentrated load  $\bar{Q}$  as

$$A_1 \bar{Q}^2 + B_1 \bar{Q} + C_1 = 0, \quad (52)$$

where the coefficients  $A_1$ ,  $B_1$ , and  $C_1$  are given by

$$A_1 = \frac{1}{4\beta_e^4} \left( 3 - 3 \frac{\tan \beta_e}{\beta_e} + \tan^2 \beta_e \right), \quad B_1 = \frac{1}{\beta_e^4} \left( \frac{1}{\cos \beta_e} - 1 - \frac{\beta_e \tan \beta_e}{2 \cos \beta_e} \right), \quad (53)$$

and

$$C_1 = \frac{\beta_e^2}{\lambda_e^2} + \frac{1}{4\beta_e^2} \left( \sec^2 \beta_e - \frac{\tan \beta_e}{\beta_e} \right) - \frac{1}{6} + \frac{A_c E_{ec} \epsilon_{sh}}{\Theta^2 (A_s E_s + A_c E_{ec})} \quad (54)$$

for pin-ended arches; and

$$A_1 = \frac{1}{2\beta_e^4} \left[ 1 + \frac{\beta_e - 3 \sin \beta_e}{\beta_e (1 + \cos \beta_e)} \right], \quad B_1 = \frac{\sin \beta_e - \beta_e}{2\beta_e^3 (1 + \cos \beta_e)}, \quad (55)$$

and

$$C_1 = \frac{\beta_e^2}{\lambda_e^2} + \frac{\cot \beta_e (\beta_e \cot \beta_e - 1)}{4\beta_e} + \frac{1}{12} + \frac{A_c E_{ec} \epsilon_{sh}}{\Theta^2 (A_s E_s + A_c E_{ec})} \quad (56)$$

for fixed arches, in which  $\lambda_e$  is the time-dependent modified slenderness of a CFST arch and is defined by

$$\lambda_e = \frac{\Theta S}{2 r_e}, \quad (57)$$

which is the product of a quarter of included angle  $\Theta/2$  with the slenderness  $S/r_e$ .

The time-dependent non-linear radial displacements given by Eqs. (47) and (48) are compared with their linear counterparts given by Eqs. (19) and (27) in Figs. 2a and 2b for pin-ended and fixed CFST arches, respectively, where the Young's

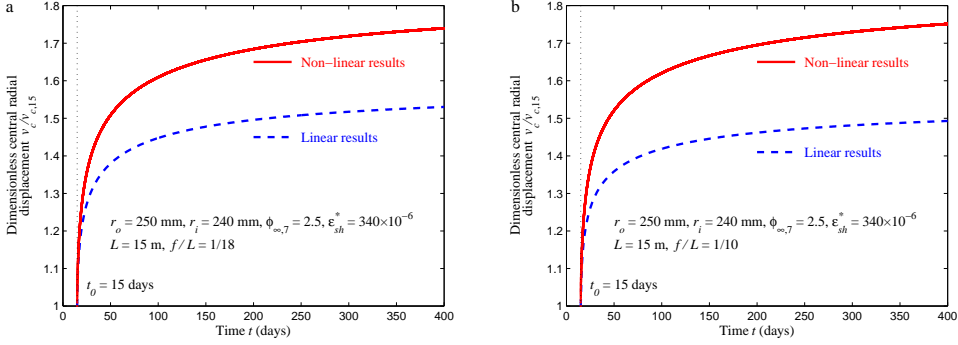


Figure 2: Comparison of non-linear and linear time-dependent central radial displacements (a. pin-ended arch and b. fixed arch).

moduli of the steel and concrete were assumed as  $E_s = 200$  Gpa and  $E_c = 30$  Gpa, a steel circular tube with outer and inner radii:  $r_o = 250$  mm and  $r_i = 240$  mm was used, the span of the arch is  $L = 15$  m,  $v_{c,15}$  is the central radial displacement at the first loading time  $t_0 = 15$  days, and the final shrinkage strain  $\epsilon_{sh} = 340 \times 10^{-6}$  and the final creep coefficient  $\phi_u = 2.29$  were adopted. The constant sustained concentrated load was assumed as  $Q = 0.1N_p$  and  $0.13N_f$  for pin-ended and fixed CFST arches respectively.

It can be seen from Figs. 2a and 2b that, as time  $t$  increases, creep and shrinkage effects result in significant increases of the radial displacements of CFST arches. It can also be seen that the increases of the time-dependent radial displacements predicted by the non-linear analysis are much greater than those predicted by the linear analysis. Hence, the linear analysis is not adequate in predicting the time-dependent radial displacements.

The non-linear time-dependent axial compressive force  $N$  is constant along the arch length and can be obtained from Eq. (52) as

$$N = -(A_s E_s + A_c E_{ec}) \Theta^2 \left\{ \frac{1}{4\beta_e^2} \left( \sec^2 \beta_e - \frac{\tan \beta_e}{\beta_e} \right) - \frac{1}{6} + \frac{A_c E_{ec} \epsilon_{sh}}{\Theta^2 (A_s E_s + A_c E_{ec})} + A_1 \bar{Q}^2 + B_1 \bar{Q} \right\} \quad (58)$$

for pin-ended arches with  $A_1$  and  $B_1$  being given by Eq. (53); and

$$N = -(A_s E_s + A_c E_{ec}) \Theta^2 \left\{ \frac{\cot \beta_e (\beta_e \cot \beta_e - 1)}{4\beta_e} + \frac{1}{12} + \frac{A_c E_{ec} \epsilon_{sh}}{\Theta^2 (A_s E_s + A_c E_{ec})} + A_1 \bar{Q}^2 + B_1 \bar{Q} \right\} \quad (59)$$

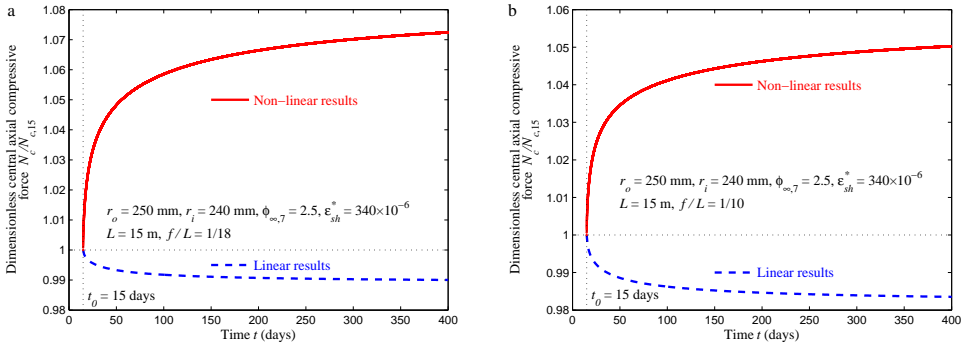


Figure 3: Comparison of non-linear and linear time-dependent axial compressive forces (a. pin-ended arch and b. fixed arch).

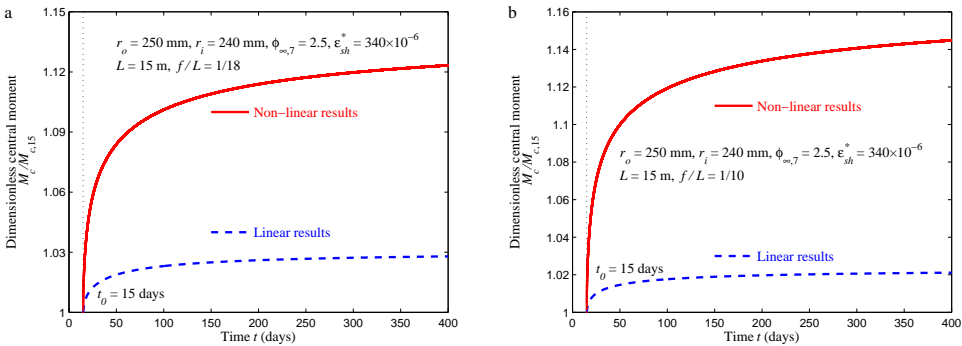


Figure 4: Comparison of non-linear and linear central moments (a. pin-ended arch and b. fixed arch).

for fixed arches with  $A_1$  and  $B_1$  being given by Eq. (55).

The bending moment in the CFST arch can be obtained by substituting Eqs. (47) and (48) into Eq. (41) as

$$M = \frac{E_s I_s + E_{ec} I_c}{R} \left\{ \left( \frac{\cos \mu_e \theta}{\cos \beta_e} - 1 \right) - \frac{\bar{Q}}{\beta_e} [\tan \beta_e \cos \mu_e \theta - H(\theta) \sin \mu_e \theta] \right\} \quad (60)$$

for pin-ended arches; and

$$M = \frac{E_s I_s + E_{ec} I_c}{R} \left\{ \beta_e \frac{\cos \mu_e \theta}{\sin \beta_e} - 1 - \frac{\bar{Q}}{\beta_e} \left[ \tan \frac{\beta_e}{2} \cos \mu_e \theta - H(\theta) \sin \mu_e \theta \right] \right\} \quad (61)$$

for fixed arches.

The time-dependent non-linear axial force and central bending moment are compared with their linear counterparts in Figs. 3 and 4, where  $N_{c,15}$  and  $M_{c,15}$  are the central axial compressive force and central moment at time  $t_0 = 15$  days. It can be seen that the non-linear analysis predicts about 7.2% and 5% increase of the time-dependent axial compressive forces  $N$  of the pin-ended and fixed CFST arch after 400 days respectively while the linear analysis predicts slight decreases of the axial force. It can also be seen that the increase of time-dependent bending moment  $M$  evaluated by the non-linear analysis is much higher than that of the linear analysis. This indicates that the time-dependent linear analysis underestimates the increases of the internal forces and may lead to an unsafe design of CFST arches.

### 5 Time-dependent limit point buckling

From viewpoint of mathematics, the limit points of a CFST arch are the local extrema of the non-linear equilibrium path, so that differentiating Eq. (52) with respect to  $\beta_e$  leads to the equilibrium equation between the dimensionless load  $\bar{Q}$  and the axial force parameter  $\beta_e$  at the limit points as

$$A_2\bar{Q}^2 + B_2\bar{Q} + C_2 = 0 \quad (62)$$

where the coefficients  $A_2$ ,  $B_2$  and  $C_2$  are given by

$$A_2 = \frac{1}{8\beta_e^4} \left[ (7 - 2\beta_e \tan \beta_e) \sec^2 \beta_e - \frac{15 \tan \beta_e}{\beta_e} + 8 \right], \quad (63)$$

$$B_2 = \frac{1}{4\beta_e^4} \left[ (8 - 5\beta_e \tan \beta_e) \sec \beta_e + \beta_e^2 (1 + \sin^2 \beta_e) \sec^3 \beta_e - 8 \right], \quad (64)$$

$$C_2 = \frac{1}{8\beta_e^2} \left[ (3 - 2\beta_e \tan \beta_e) \sec^2 \beta_e - 3 \frac{\tan \beta_e}{\beta_e} \right] - \frac{\beta_e^2}{\lambda^2} \quad (65)$$

for pin-ended arches; and

$$A_2 = 2A_1 + \frac{3(\beta_e - \sin \beta_e)}{4\beta_e^5(1 + \cos \beta_e)} - \frac{\sin \beta_e}{4\beta_e^3(1 + \cos \beta_e)^2}, \quad (66)$$

$$B_2 = \frac{3B_1}{2} + \frac{\sin \beta_e}{4\beta_e(1 + \cos \beta_e)^2}, \quad (67)$$

$$C_2 = \frac{\beta_e \cos \beta_e}{4 \sin^3 \beta_e} - \frac{1}{8 \sin^2 \beta_e} - \frac{\cot \beta_e}{8 \beta_e} - \frac{\beta_e^2}{\lambda_e^2} \quad (68)$$

for fixed arches.

The limit point buckling loads  $\bar{Q}$  and the corresponding axial force parameters  $\beta_e$  for a given CFST arch at a specified time  $t$  can then be obtained by solving Eqs. (52) and (62) simultaneously. The corresponding radial displacement  $v$  can also be obtained by substituting the obtained load  $\bar{Q}$  and axial force parameter  $\beta_e$  into Eq. (47) or (48).

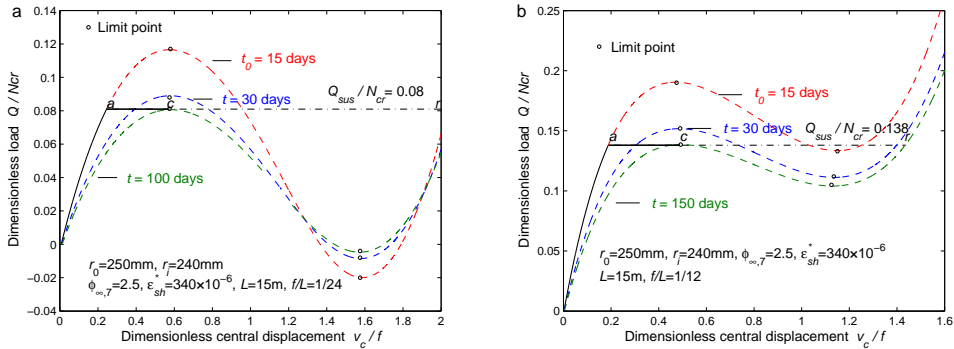


Figure 5: Non-linear time-dependent central displacements for limit point buckling of CFST arches (a. pin-ended arch and b. fixed arch).

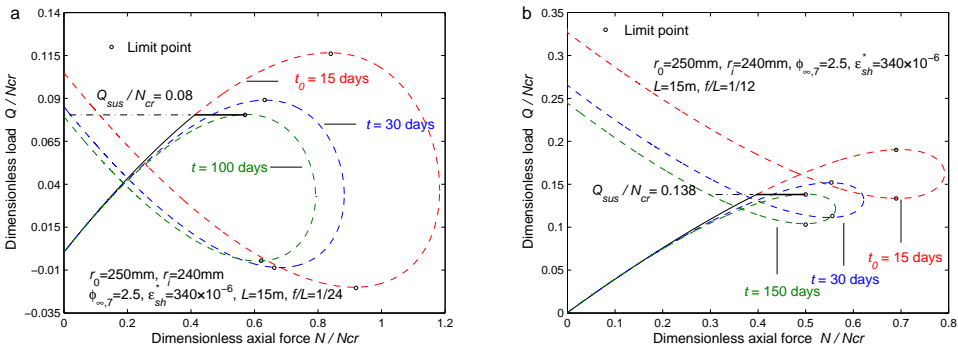


Figure 6: Non-linear time-dependent axial compressive forces for limit point buckling of CFST arches (a. pin-ended arch and b. fixed arch).

The non-linear equilibrium paths at different times are shown in Fig. 5a for a pin-ended CFST arch and in Fig. 5b for a fixed CFST arch as variations of the dimensionless central radial displacement  $v_c/f$  with the dimensionless radial load  $Q/N_{cr}$ ,

and also shown in Figs. 6a and 6b as variations of the dimensionless axial compressive force  $N/N_{cr}$  with the dimensionless load  $Q/N_{cr}$ , where  $N_{cr}$  is the second buckling load of the corresponding CFST columns ( $N_{cr} = N_P$  for pin-ended arches and  $N_{cr} = N_F$  for fixed arches given by Eq. (50)). It can be seen that when time  $t_0 = 15$  days and  $t = 30$  days, the equilibrium of both arches are on the stable branches and the limit buckling loads of both pin-ended and fixed CFST arches are much higher than the sustained load  $Q_{sus} = 0.08N_P$  for the pin-ended arch and  $Q_{sus} = 0.138N_F$  for the fixed arch. Hence, the arches cannot buckle under the sustained load  $Q_{sus}$  at time  $t_0 = 15$  days and  $t = 30$  days. However, when time  $t = 100$  days for pin-ended arch and  $t = 150$  days for the fixed arch, their limit point buckling loads decrease and are equal to the sustained loads  $Q_{sus}$ . At the same time, owing to creep of the concrete core, the crown of the arch displaces from the position  $a$  at time  $t_0 = 15$  days to the position  $c$  at time  $t = 100$  days for the pin-ended arch and at time  $t = 150$  days for the fixed arch as shown by the solid coarse line. In these cases, the critical equilibrium at the upper limit points is attained and the CFST arches may fail in a limit point buckling mode. Because in practice, sustained loads do not change during buckling and so deformations of CFST arches cannot follow the non-linear equilibrium path (dashed lines), but will suddenly snap-through from the limit point to an equilibrium point  $r$  on the remote equilibrium branch as shown by the horizontal dotted-dashed line.

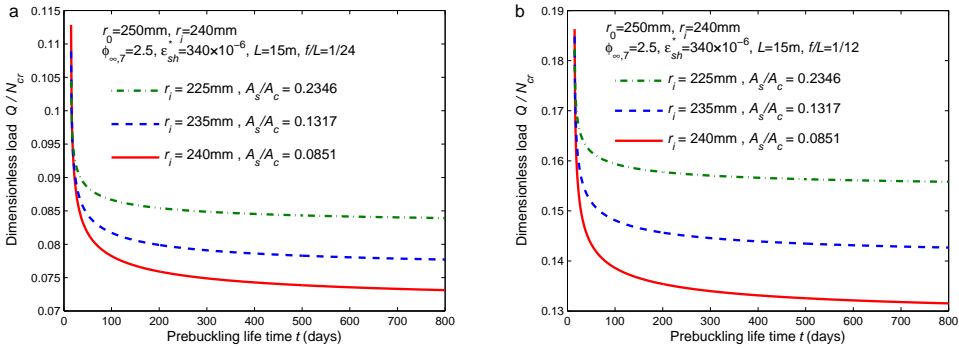


Figure 7: Prebuckling life time for limit point buckling of CFST arches (a. pin-ended arch and b. fixed arch).

The prebuckling structural life time of CFST arches for the time-dependent limit point buckling of CFST arches can be determined by using Eqs. (52) and (62). A typical structural life time prior to limit point buckling is shown in Fig. 7, which demonstrate that the prebuckling structural life time  $t$  increases as the dimensionless sustained load  $Q/N_{cr}$  decreases. When the sustained load is sufficiently low,

the limit point buckling does not occur, whereas for a higher sustained load, the prebuckling structural life is rather short. In the first 130 days of structural life, the decrease of the sustained load for the limit point buckling is quite rapid but becomes slow in the following days. Under the same sustained load, the prebuckling structural life time increases with the increase of the area ratio of the steel tube to the concrete core ( $A_s/A_c$ ).

## 6 Time-dependent bifurcation buckling

It has been shown [Bradford, Uy, and Pi (2002); Pi, Bradford, and Uy (2002); Pi, Bradford, and Qu (2011)] that when  $\mu_e\Theta = \pi$  or  $\mu_e\Theta \approx 1.4303\pi$ , a circular arch may buckle in an antisymmetric bifurcation mode. Substituting these into Eq. (52) leads to the equation for the time-dependent antisymmetric bifurcation buckling load  $Q_b$  as

$$3\bar{Q}_b^2 - 8\bar{Q}_b + \pi^2 - \frac{2\pi^4}{3} + \frac{4\pi^6}{\lambda_e^2} + \frac{4\pi^4 A_c E_{ec} \epsilon_{sh}}{\Theta^2 (A_s E_s + A_c E_{ec})} = 0 \quad (69)$$

for pin-ended arches; and

$$6.22\bar{Q}_b^2 - 13.98 \times (1.4303\pi)\bar{Q}_b + \frac{(1.4303\pi)^4}{3} + \frac{4 \times (1.4303\pi)^6}{\lambda_e^2} + \frac{4\pi^4 A_c E_{ec} \epsilon_{sh}}{\Theta^2 (A_s E_s + A_c E_{ec})} = 0 \quad (70)$$

for fixed arches.

Typical time-dependent non-linear bifurcation buckling behaviour obtained from Eq. (69) is displayed in Figs. 8a and 8b for a pin-ended CFST arch. The fine solid line represents the short-term equilibrium path up to a sustained load  $Q_{sus}/N_{cr} = 0.184$  for the pin-ended arch while the coarse solid line denotes the time-dependent equilibrium path of the arch due to creep and shrinkage of its concrete core under the sustained load. The dashed lines describe the non-linear equilibrium path given by Eqs. (47) and (52) for different times. The corresponding limit point loads are marked as hollow small circles while the bifurcation buckling loads obtained from Eqs. (47) and (69) are marked as hollow small squares.

It can be seen from Figs. 8a and 8b that the bifurcation buckling load of the pin-ended CFST arch decreases with an increase of time. At time  $t = 15$  days and  $t = 30$  days, the sustained load  $Q_{sus}/N_{cr}$  is lower than the bifurcation buckling load and so the arch is in a stable equilibrium state. The radial displacement increases from the position  $a$  at the time  $t_0 = 15$  days to the position  $c$  at time  $t = 200$  days, at which time the sustained load equals the upper bifurcation buckling load. Hence, the

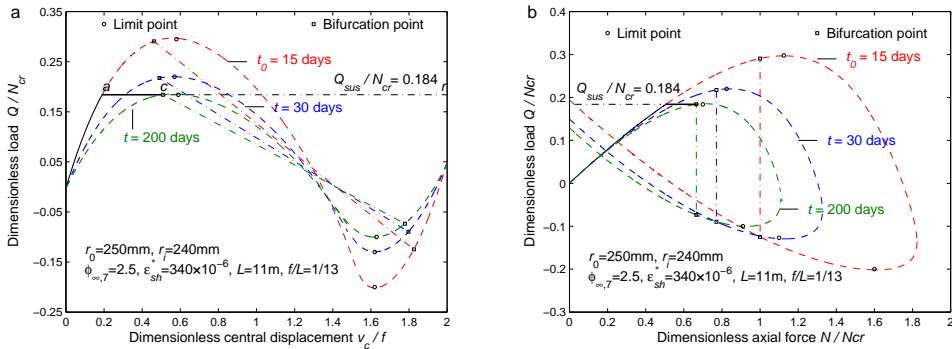


Figure 8: Non-linear time-dependent equilibrium for bifurcation buckling of CFST pin-ended arches.

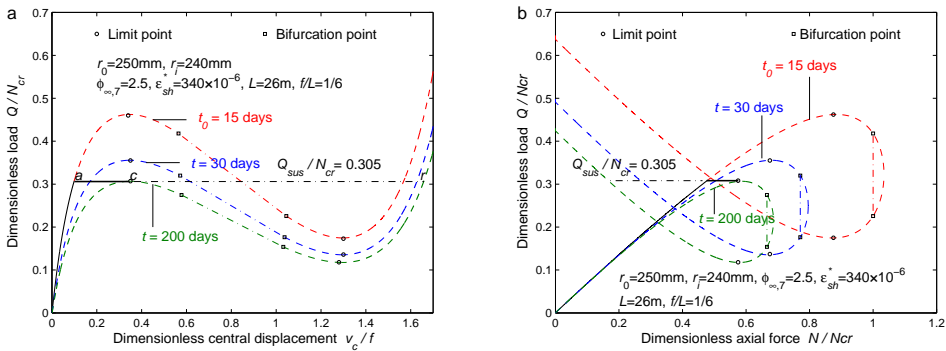


Figure 9: Non-linear time-dependent equilibrium for bifurcation buckling of CFST fixed arches.

arch may fail in a time-dependent bifurcation buckling mode at time  $t = 200$  days. Because the upper limit point buckling load is higher than the upper bifurcation buckling load, the time-dependent bifurcation buckling will occur first. Similar to the counterparts of limit point buckling, the sustained load remains constant after bifurcation buckling, so the CFST arch cannot follow the secondary post-bifurcation equilibrium path shown by the fine dotted-dashed lines and the lower bifurcation point cannot be reached. The equilibrium configuration of the arch will suddenly jump from the bifurcation point to a remote stable equilibrium point.

Although CFST pin-ended arches can buckle in a time-dependent bifurcation mode, CFST fixed arches cannot buckle in a time-dependent bifurcation mode as shown in Figs. 9a and 9b. It can be seen from Figs. 9a and 9b that the bifurcation points

are located on the descending unstable equilibrium branches after the upper limit points. Hence, the bifurcation point cannot be reached during the time-dependent deformation. However, the time-dependent limit point can be reached if the sustained load is sufficiently high ( $Q_{sus}/N_{cr} = 0.305$  for the arch in Figs. 9a and 9b) and the time is sufficiently long ( $t = 200$  days). It can be concluded that CFST fixed arches under a sustained central concentrated load can buckle in a time-dependent limit point instability mode, but not in a time-dependent bifurcation mode.

The structural life time of CFST pin-ended arches prior to time-dependent bifurcation buckling can be obtained from Eq. (69) as shown in Fig. 10. It can be seen that in the first 100 days of structural life time, the sustained load for the time-dependent bifurcation buckling decreases rapidly but becomes slow in the following days, and that the area ratio of the steel tube to the core concrete influences the creep buckling loads significantly. The dimensionless creep buckling load decreases with a decrease of the ratio  $A_s/A_c$ .

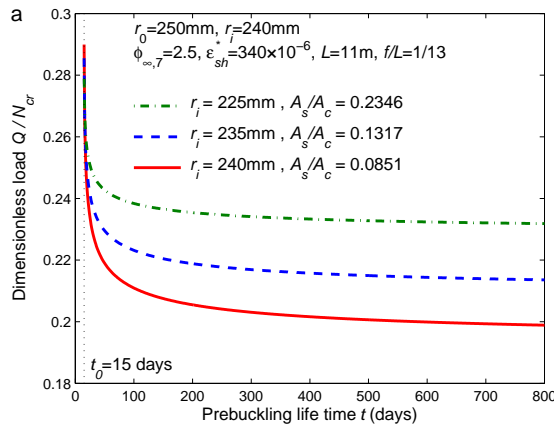


Figure 10: Prebuckling life for bifurcation buckling of pin-ended CFST arches.

## 7 Modified slenderness for time-dependent buckling mode switches

Because a CFST pin-ended arch may buckle in an time-dependent limit point instability mode or in an time-dependent bifurcation mode, for a given CFST arch, it needs to determine whether the limit point instability mode or the bifurcation mode is dominant. It has been shown [Pi, Bradford, and Qu (2011)] that the modified slenderness of an arch plays a key role in determining the dominant buckling mode. The modified slenderness  $\lambda_{e, sb}$  defining the switch between the limit point

and bifurcation buckling modes for pin-ended arches can be obtained by solving Eqs. (52) and (62) simultaneously when  $Q_s = Q_b$  and  $\mu_e \Theta = \pi$ , which leads to  $\lambda_{e, sb} \approx 9.8$ . For pin-ended CFST arches with  $\lambda_e \leq \lambda_{e, sb}$  at time  $t$ , limit point buckling is the dominant buckling mode. When  $\lambda_e \geq \lambda_{e, sb}$  at time  $t$ , bifurcation is the dominant buckling mode because the corresponding limit point buckling load is higher. However, for fixed CFST arches, the limit point buckling mode governs their time-dependent buckling under a central concentrated load [Bradford, Uy, and Pi (2002)].

It has also been shown [Bradford, Uy, and Pi (2002)] that very shallow CFST arches do not have typical buckling phenomena. The modified slenderness of a CFST arch can also be used to define the switch between arches with time-dependent buckling phenomena and arches without time-dependent buckling phenomena. To determine the time-dependent arch modified slenderness  $\lambda_{e, ns}$  for the switch, the dimensionless central radial displacement corresponding to the lowest possible buckling load can be used, which are given by

$$\lim_{\mu_e \Theta \rightarrow \pi/2} \tilde{v}_c = \frac{S^2}{\pi^2 R^2} \left( 1 - \frac{2}{\pi} + \frac{\pi^2}{8} - \frac{\pi}{2} \pm \sqrt{\frac{4}{\pi^2} + \frac{8}{\pi} + \frac{\pi^2}{6} - 3 - \frac{\pi^4}{4\lambda_e^2}} \right) \quad (71)$$

for pin-ended arches, and

$$\lim_{\mu_e \Theta \rightarrow \pi} \tilde{v}_c = \frac{S^2}{\pi^2 R^2} \left( 1 \pm \sqrt{1 - \frac{\pi^2}{48} - \frac{\pi^4}{\lambda_e^2}} \right) \quad (72)$$

for fixed arches.

The existence of real solutions of Eqs. (71) and (72) leads to the time-dependent arch modified slenderness  $\lambda_{e, ns}$  for the switch between buckling and no buckling as [Bradford, Uy, and Pi (2002)]

$$\lambda_{e, ns} = 3.91 \quad \text{and} \quad \lambda_{e, ns} = 11.07 \quad (73)$$

for CFST pin-ended and fixed arches, respectively.

The typical relationship between the time-dependent arch modified slenderness with time for a CFST pin-ended arch is illustrated in Fig. 11, which shows that the modified slenderness  $\lambda_e$  of the CFST arch decreases as time increases and the increase is rapid in the first 100 days after concrete core casting. Consequently, for a CFST arch with a modified slenderness  $\lambda_e \geq \lambda_{e, sb}$  at time  $t_1$ , its modified slenderness may become lower than  $\lambda_{e, sb}$  ( $\lambda_e \leq \lambda_{e, sb}$ ) at the later time  $t_2 > t_1$ , which indicates that the dominant buckling mode of the CFST arch is of bifurcation at time  $t_1$  while its dominant buckling mode is of limit point instability.

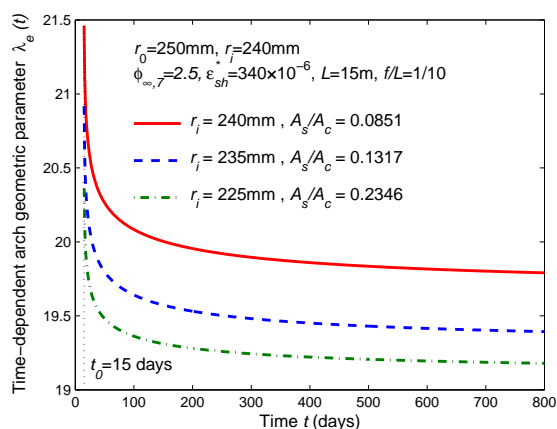


Figure 11: Variations of modified slenderness of a CFST arch with time.

## 8 Comparison with finite element results

### 8.1 Finite element model

The analytical solutions for the time-dependent structural behaviour of CFST arches are herein compared with the finite element (FE) results of the commercial FE package ANSYS. In the ANSYS FE computation, a CFST arch is modeled by the beam188 element with a solid section for the concrete core and a tube section for the steel tube as shown in Fig. 12. In a global cylindrical coordinate system, the FE model has 161 nodes and 160 elements. It is known that ANSYS treats one element with two different sections as two component elements bonded together. Hence, 320 component elements are generated by ANSYS. In the ANSYS computation, the component elements between two nodes are treated to be bonded together as a single element. The material properties of concrete and steel were assigned to the solid section and to the tube section, respectively.

Although ANSYS provides 13 implicit creep equations for users to model creep behaviour of metal, there is no suitable model that is consistent with the age-adjusted effective modulus method and that can be used directly to account for creep of the concrete core. Hence, to account for the creep and shrinkage of the concrete core, the user-programmable features (UPFs) of ANSYS was used to redefine the user-defined creep law in the subroutine usercreep.F provided by ANSYS and to add the time-dependent shrinkage strain in the subroutine, which will compute the time-dependent creep and shrinkage strain at each time step. In the revised program, the time domain is defined in days. For the time-dependent linear analysis of a CFST

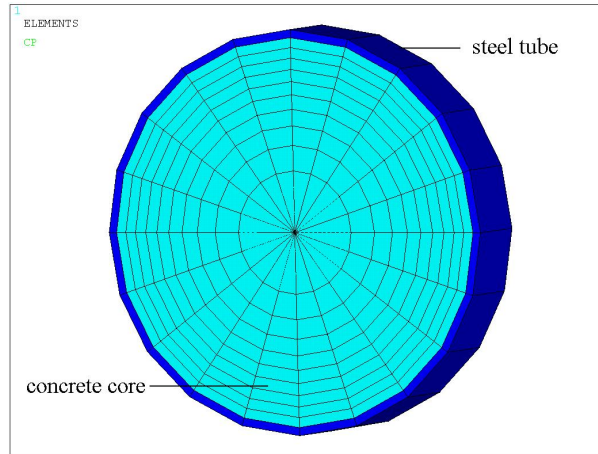


Figure 12: Section of finite element model in ANSYS.

arch under a sustain load, the sustain load is assigned and the time-dependent analysis is turned on, the effect of the creep and shrinkage is computed at each time step. For the time-dependent non-linear analysis of a CFST arch under a sustained load, for each time step, the incremental-iterative solutions based on the Newton-Raphson approach and the arc-length method are carried out with load increments until the sustained load is attained. In ANSYS, the load steps and convergence criterion are automatically assigned when the non-linear analysis is turned on.

## 8.2 Comparison with finite element results for time-dependent displacements

The analytical solutions for the time-dependent linear and non-linear radial displacement of CFST arches given by Eqs. (19) and (47) are compared with its FE counterparts in Fig. 13 as variations of dimensionless central radial displacement  $v_c/f$  with time  $t$ , where the outer and inner radii of the steel tube were  $r_o = 250$  mm and  $r_i = 240$  mm, the span of the arch was  $L = 18$  m, the rise-to-span ratio was  $f/L = 1/30$ , and the arch was assumed to be pin-ended. In the computation, Young's moduli of the steel and concrete were assumed as  $E_s = 200$  Gpa and  $E_c = 30$  Gpa, respectively, and the sustained concentrated load was assigned as  $Q = 0.05N_p$ . It can be seen from Fig. 13 that the analytical solutions almost coincide with the FE results and that the time-dependent non-linear radial displacements are indeed much larger than their linear counterparts.

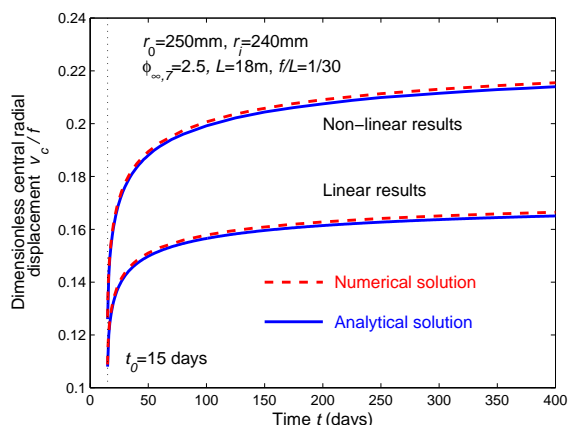


Figure 13: Comparison of analytical and FE solutions of time-dependent central radial displacements.

### 8.3 Comparison with finite element results for time-dependent stresses

The time-dependent stresses in both the steel tube and the concrete core predicted by linear analytical solution are compared with their FE counterparts in Fig. 14 for a pin-ended CFST arch as variations of the stresses  $\sigma_s$  at the top of the steel tube and  $\sigma_c$  at the top of the concrete with time  $t$ , where the outer and inner radii of the circular steel tube were  $r_0 = 250$  mm and  $r_i = 225$  mm (or  $r_i = 240$  mm), the span of the arch was  $L = 15$  m, and the rise-to-span ratio was  $f/L = 1/6$ . The constant sustained concentrated load is assumed as  $Q = 0.07N_p$  while the Young's moduli of the steel and concrete were assumed the same as the previous example.

Fig. 14 shows that the analytical solutions agree with the FE results very well and that in the long-term, the creep and shrinkage of the concrete core cause an increase of compressive stress in steel tube and a decrease of compressive stresses in concrete core. The increase of the compressive stresses in the steel tube with  $r_i = 240$  mm is much more than those with  $r_i = 225$  mm.

### 8.4 Comparison with finite element results for time-dependent non-linear buckling

The FE model was also used for the time-dependent non-linear buckling analysis of a pin-ended CFST arch. The steel tube of the arch cross-section was assumed to have the outer and inner radii of  $r_0 = 250$  mm and  $r_i = 240$  mm. The span of the arch was  $L = 11$  m and the rise-to-span ratio was  $f/L = 1/24$ . A sustained

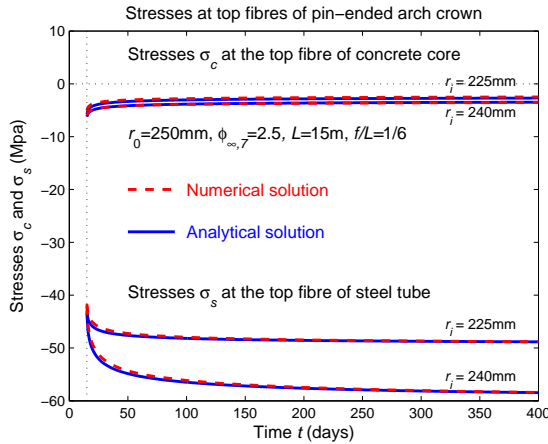


Figure 14: Comparison of analytical and numerical solutions of time-dependent stresses at top fibres of shallow pin-ended CFST arch crown.

radial concentrated load  $Q = 0.07N_p$  was applied at the crown of the arch. The FE results are compared with the analytical solutions obtained from Eqs. (47) and (52) are shown in Fig. 15 as variations of the dimensionless central radial load  $\bar{Q}$  with the dimensionless central displacement  $v_c/f$ , where the dimensionless load  $\bar{Q}$  was calculated using Eq. (49).

The non-linear analysis was performed at the each time step from time  $t_0 = 15$  days until the sustained load is attained. The equilibrium path under the sustained load is shown by the red dashed line and the non-linear equilibrium paths at  $t_0 = 15$  days and  $t = 100$  days are shown in the green dashed lined in Fig. 15. The analytical solutions for the non-linear equilibrium paths was also performed as shown by the black solid line Fig. 15 and the analytical solution for equilibrium under the sustained load is shown by the blue solid line. The sustained load was compared with the possible buckling load at each time step. It was found that the limit point buckling load at time  $t = 100$  days is equal to the sustained load. Hence, although the arch cannot buckle when the sustained load  $Q = 0.07N_p$  is applied at time  $t_0 = 15$  days, it may buckle in the long-term at time  $t = 100$  days. Comparison of the analytical solutions with the FE results shows that they agree with each other for the time-dependent equilibrium under the sustained load, for the non-linear equilibrium paths at each time step, and for the time-dependent limit point buckling load.

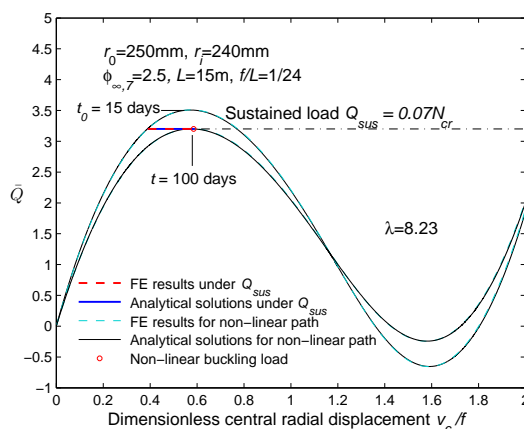


Figure 15: Comparison of analytical and numerical solutions of time-dependent buckling behaviour of shallow pin-ended CFST arches.

## 9 Conclusions

This paper investigated the time-dependent linear and non-linear in-plane structural and buckling behaviour of shallow CFST arches subjected to a sustained central concentrated radial load. Linear and non-linear analytical solutions for the time-dependent displacements and internal actions and for the time-dependent limit point and bifurcation buckling were derived. It has been found that creep and shrinkage of concrete core have significant effects on the time-dependent non-linear deformations, internal forces and buckling behaviour of shallow CFST arches. Comparisons between the linear and non-linear analyses demonstrate that the linear analysis is not adequate for predicting the time-dependent structural behaviour of shallow CFST arches. The linear predictions for the displacement and internal actions are much smaller than the counterparts predicted by the non-linear analysis. Due to the visco-elastic effects of creep and shrinkage of the concrete core, the equilibrium state of a shallow CFST arch becomes time-dependent. The stable equilibrium state of a CFST arch at an early time  $t_1$  under a sustained central radial load may change to a critical equilibrium state when the time is sufficiently long and the load is sufficiently large, and thus the arch may buckle at a later time  $t_2$ . The solutions for the possible structural life time of a shallow CFST arch prior to buckling were also derived for assessing the influence of various parameters on the time-dependent non-linear structural and buckling behaviour of shallow CFST arches. The creep and shrinkage of the concrete core reduces the safety margins

of the serviceability limit state and even the strength limit state of shallow CFST arches.

The analytical solutions were compared with the FE results of ANSYS, which shows that the agreement between them is very good.

**Acknowledgement:** This work has been supported by the Australian Research Council through Discovery Projects.

## References

**Abdulrazeg, A. A.; Noorzaei, J.; Khanehzaei, P.; Jaafar, M. S.; Mohammed, T. A.** (2010): Effect of Temperature and Creep on Roller Compacted Concrete Dam During the Construction Stages. *CMES: Computer Modeling in Engineering & Sciences*, vol. 68, no. 3, pp. 239–268.

**ACI Committee-209** (1982): *Prediction of Creep, Shrinkage and Temperature Effects in Concrete Structures*. American Concrete Institute(ACI), Detroit.

**AS3600** (2009): *Australia Standard: Concrete Structures*. Standard Association of Australia, Sydney.

**Bazant, Z. P.** (1972): Prediction of concrete creep effects using age-adjusted effective modulus method . *ACI Structural Journal*, vol. 69, no. 4, pp. 212–217.

**Bazant, Z. P.; Cedolin, L.** (2003): *Stability of structures*. Mineola, N.Y. : Dover Publications.

**Bradford, M. A.; Pi, Y.-L.; Qu, W.-L.** (2011): Time-dependent in-plane behaviour and buckling of concrete-filled steel tubular arches . *Engineering Structures*, vol. 33, pp. 1781–1795.

**Bradford, M. A.; Uy, B.; Pi, Y.-L.** (2002): In-plane elastic stability of arches under a central concentrated load . *Engineering Structures*, vol. 128, no. 7, pp. 710–719.

**Branson, D. E.** (1977): *Deformation of Concrete Structures* . New York : McGraw-Hill.

**Chen, B. C.** (2000): Experimental study on mechanical behaviours of concrete-filled steel tubular rib arch under in-plane loads. *Engineering Mechanics*, vol. 17, no. 2, pp. 44–50.

**Ferretti, E.; Di Leo, A.** (2008): Cracking and Creep Role in Displacements at Constant Load: Concrete Solids in Compression. *CMES: Computer Modeling in Engineering & Sciences*, vol. 7, no. 2, pp. 59–80.

- Gilbert, R. I.; Ranzi, G.** (2011): *Time-dependent behaviour of concrete structures*. London ; New York : Spon.
- Han, L. H.; Yang, Y. F.; Liu, W.** (2004): The behaviour of concrete-filled steel tubular columns with rectangular section under long-term loading . *Journal of Civil Engineering*, vol. 37, no. 3, pp. 12–18.
- Pi, Y.-L.; Bradford, M. A.** (2009): Non-linear in-plane postbuckling of arches with rotational end restraints under uniform radial loading . *International Journal of Non-linear Mechanics*, vol. 44, no. 9, pp. 975–89.
- Pi, Y.-L.; Bradford, M. A.; Qu, W.-L.** (2011): Long-term non-linear behaviour and buckling of shallow concrete-filled steel tubular arches . *International Journal of Non-linear Mechanics*, vol. 46, pp. 1155–1166.
- Pi, Y.-L.; Bradford, M. A.; Tin-Loi, F.** (2007): Non-linear analysis and buckling of elastically supported circular shallow arches . *International Journal of Solids and Structures*, vol. 44, no. 7-8, pp. 2401–2425.
- Pi, Y.-L.; Bradford, M. A.; Tin-Loi, F.; Gilbert, R. I.** (2007): Geometric and material nonlinear analysis of elastically restrained arches . *Engineering Structures*, vol. 29, no. 3, pp. 283–295.
- Pi, Y.-L.; Bradford, M. A.; Uy, B.** (2002): In-plane stability of arches . *International Journal of Solids and Structures*, vol. 39, pp. 105–125.
- Pi, Y.-L.; Liu, C. Y.; Bradford, M. A.; Zhang, S. M.** (2012): In-plane strength of concrete-filled steel tubular circular arches . *Journal of Constructional Steel Research*, vol. 69, pp. 77–94.
- Pi, Y.-L.; Trahair, N. S.** (1998): Non-linear buckling and postbuckling of elastic arches . *Engineering Structures*, vol. 20, no. 7, pp. 571–579.
- Terrey, P. J.; Bradford, M. A.; Gilbert, R. I.** (1994): Creep and shrinkage of concrete in concrete-filled circular steel tubes . In *Proceeding of 6th International Symposium on Tubular Structures*, pp. 293–298.
- Uy, B.** (2001): Static long-term effects in short concrete-filled steel box columns under sustained loading . *ACI Structural Journal*, vol. 98, no. 1, pp. 96–104.
- Wang, T.; Bradford, M. A.; Gilbert, R. I.** (2005): Creep buckling of shallow parabolic concrete arches . *Journal of Structural Engineering ASCE*, vol. 132, no. 10, pp. 1641–1649.
- Zhong, S. T.** (1994): *Concrete-filled Steel Tubular Structures* . Heilongjiang Science and Technology Press.